Astron. Astrophys. 360, L9–L12 (2000)

ASTRONOMY AND ASTROPHYSICS

LETTER

Letter to the Editor

The structure and momentum of multiple collimated outflows in the protoplanetary nebula Frosty Leo

R. Sahai[1], V. Bujarrabal[2], A. Castro-Carrizo[2], and A. Zijlstra[3]

[1] California Institute of Technology, Jet Propulsion Laboratory, MS 183-900, Pasadena, CA 91109, USA
[2] Observatorio Astronómico Nacional, Ap. 1143, 28800 Alcalá de Henares, Spain
[3] UMIST, Department of Physics, PO Box 88, Manchester M60 1QD, UK

Received 26 April 2000 / Accepted 26 June 2000

Abstract. We have discovered multiple jet-like features in the inner regions of the protoplanetary nebula (PPN) Frosty Leo, in optical images obtained with the Hubble Space Telescope. Frosty Leo is only the second PPN (after CRL2688) and the first oxygen-rich one, to show well-focussed jets close to the equatorial plane. The nebula consists of two bright compact structures embedded inside two large tenuous bubbles, separated by a flaring, roughly edge-on disk. The relatively high surface brightnesses of two ansae and substructures in the jets imply that the latter have carved out holes in the optically thick central region of the nebula, allowing starlight to escape with very little attenuation. Millimeter-wave CO line observations with the IRAM 30m radiotelescope show the presence of slow ($\sim$10 km s^{-1}) and fast ($>$50 km s^{-1}) components in a molecular outflow associated with the bright inner ($< 10''$) regions of the nebula. The mechanical momentum in the fast outflow is about a factor 500 larger than that available from the stellar radiation (L/c) during the post-AGB life of the source, and most likely derives from the gravitational energy of a close binary central star.

Key words: stars: AGB and post-AGB – stars: mass-loss – ISM: reflection nebulae – ISM: individual objects:

1. Introduction

Frosty Leo (IRAS 09371+1212) is a well-known bipolar nebula around a star believed to be in the short transition phase between the AGB and planetary nebula evolutionary phases – i.e. it is a protoplanetary nebula (PPN). Forveille et al. (1987) first identified it as an evolved object with substantial CO line emission showing the presence of a dense expanding molecular envelope, and suggested the presence of water ice in its dust grains, confirmed later by e.g. Rouan et al. (1988). Optical and near-IR imaging of Frosty Leo revealed a remarkable extended point-symmetric bipolar reflection nebula with a pair of peripheral ansae and bisected by a dense disk seen edge-on (Morris & Reipurth 1990, Langill et al. 1994). Roddier et al. (1995) found a binary star at the center of the nebula from adaptive optics imaging at 1.65 μm. We report here optical imaging with the Hubble Space Telescope (HST) of Frosty Leo, revealing complex new nebular structures which have important implications for the shaping of planetary nebulae (PNe). New, sensitive millimeter-wave observations indicate a complex kinematic structure of the molecular gas. In our analysis of these data, we assume that the central star has $T_{\rm eff}$=3750K, luminosity L=250(D/kpc)$^2 L_\odot$, and is located at a distance D=3 kpc (Robinson et al. 1992, Mauron et al. 1989).

Send offprint requests to: Raghvendra Sahai

2. Observations

The Wide Field Camera (800x800 pixel^2 with a plate scale of 0.″0996/pixel) was used to image Frosty Leo through the wide-band filter F606W ($\langle\lambda\rangle$=593.5 nm, $\delta\lambda$=149.7 nm) without, and crossed with, the polarisation filter set POLQ. Since the image with no polariser has larger saturation in the bright central region, we have used a total intensity image computed from images at 3 polariser orientations [see Sahai et al. 1999a (SZBtL99)].

The mm-wave $J = 1 \rightarrow 0$ and $J = 2 \rightarrow 1$ lines of ^{12}CO and ^{13}CO were observed with the IRAM 30m radiotelescope (Pico de Veleta, Spain) during August and November 1998, using SIS receivers tuned in SSB mode, with typical system temperatures of $\sim$ 1000 K, at λ = 1.3 mm, and 500 K, at λ = 2.6 mm (in units of $T_{\rm mb}$, see below). Weather conditions were good, with zenith opacities at 230 GHz in the range 0.3-0.8. Telescope pointing was verified frequently by observing continuum sources close to our target. The spatial resolution is about 12-13″ at 1.3 mm and about 22″ at 2.6 mm. The mm-wave spectra presented here are calibrated in units of the main beam Rayleigh-Jeans-equivalent antenna temperature, $T_{\rm mb}$, using the chopper-wheel calibration method.

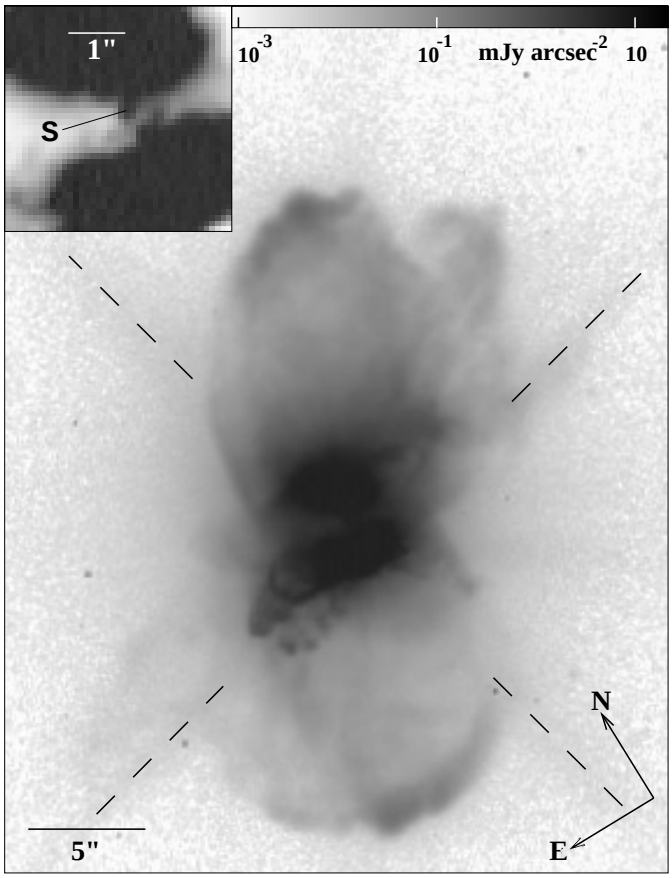

Fig. 1. Optical (0.6μm) image (reverse grey-scale image, log stretch) of the Frosty Leo nebula computed from 3 WFPC2/HST images taken through the wide-band F606W/POLQ filter/polariser. Inset shows expanded view of the nebular center. Dashed lines indicate artifacts due to the telescope optics

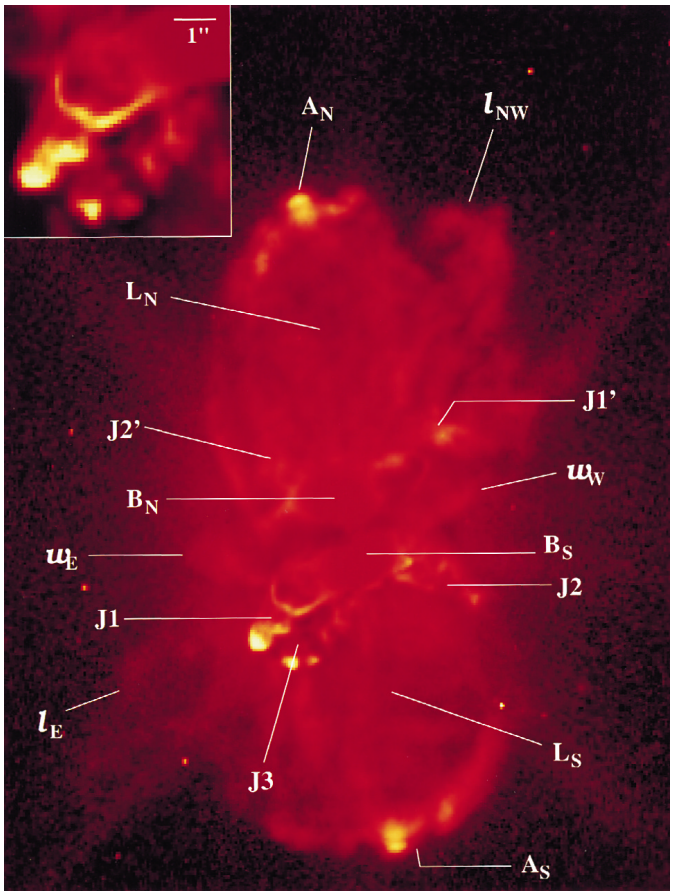

Fig. 2. A false-color image generated by processing the image in Fig. 1 in order to emphasize sharp structures. The processed image, $Im_P = Im_O/(Im_O + 0.04 Im_S)$, where Im_O is the original image, and Im_S is obtained by smoothing Im_O. Inset shows expanded view of jets J1 and J3

3. Results

3.1. Optical morphology

The F606W image of Frosty Leo (Figs. 1 & 2) shows the previously known, extended bipolar nebula in scattered light. Two large lobes (L_N and L_S) of radial extent 13.″5 separated by a relatively dark waist can be seen. The lobes are significantly limb-brightened, indicating that they are *optically-thin* bubble-like structures with relatively dense walls and a tenuous interior. The bright ansae, A_N and A_S, seen at the tips of these lobes, appear knotty, and their shapes follow the curvature of the periphery of the lobes. L_N has a higher surface brightness than L_S by a factor which decreases from about 4 at a radial offset of 6″ to 1.5 at the tips (i.e. in the ansae).

The complex inner region of Frosty Leo has several distinctive geometrical features. Two bright blobs (B_N & B_S, saturated in image), lie north and south of a narrow waist with a *flaring* disk-like structure, although it departs significantly from a smooth, symmetrical geometry – e.g. the W side of the waist is significantly narrower than the E side. A bright point-like source, S, presumably the central star, is located in the waist at the center of the nebula, and additional compact knots appear attached to the inner edge of blob B_S (inset, Fig. 1). The binary found by Roddier et al. (1995) at the center of the nebula has a separation of 0.″18, and would therefore not be well resolved in our 0.″0996 resolution HST images. However, the identical spectral type of both binary members is cause for concern that one of these may be due to light scattered off a dust condensation or an artifact of the adaptive optics technique.

Three radial jet-like structures, J1,J2, and J3, emanate from blob B_S. The brightest of these, J1, shows three substructures – a very bright tip, and two bright limb-brightened lobes. J2 is similar in overall shape and size to J1, but its substructure is less well defined. J3 consists of a chain of knots lying on the periphery of an elongated structure, roughly similar in size to J1 and J2, but with a less sharply tapered shape. Faint counterparts to J1 and J2 are marginally visible on the northern side of the nebula (labelled J1', J2'); their faintness is probably due to their location on the far-side of the nebula resulting in significant attenuation by intervening nebular dust. The collimated structures J1, J2, J3, J1' and J2' probably signify the presence of low-latitude jets. The substructures in J1 and J3 seem to show a sequence of shock fronts, that are most likely due to temporal

variations in the momentum flux of these jets. Two protrusions (w_E and w_W) appear at the periphery of the waist, and additional faint lobes (l_{NW} and l_E) extend to the NW and E.

The bipolar nebula is surrounded by a faint, roughly round halo (Langill et al. 1994). Averaging the radial intensity over large (20°-35°) angular wedges with their apex at the center, we can trace the halo out to r≈23″, where it becomes limited by background sky noise. The halo intensity, S, is well-fit by a power-law ($S \propto r^{-\alpha}$), with α ∼3.9-4.1, significantly different from the value (3) expected for scattered light in a spherical envelope characterised by (i) a constant expansion velocity and (ii) a constant mass-loss rate, $\dot{M}$. Therefore, either (i) and/or (ii) above are not true (e.g. due to an increase in $\dot{M}$ over the last 30,000 yrs), or the halo density distribution has been modified by strong shock interactions.

The ansae have peak intensities, $S_{0.6\mu m}$=0.27 (A_N) & 0.18 (A_S) mJy arcsec^{-2}, comparable to the *maximum* possible intensity of scattered light at an offset ϕ=13.″1 from the central star [given by $S_{max}=F_{0.6\mu m}/(4\pi\phi^2)$=0.32 mJy arcsec^{-2}, where $F_{0.6\mu m}$=0.69 mJy is the stellar flux density at 0.6μm]. Similarly, the two bright knots near the tip of jet J1 have peak intensities of 0.8 & 1.5 mJy arcsec^{-2}, which are only a factor 1.4-1.8 less than the theoretical maximum. Since the central region (radius $\lesssim$4″) is quite optically thick even at 1 μm (Robinson et al. 1992), we conclude that the jets which have produced the ansae and J1, have carved out holes in this region, allowing the starlight to escape with very little attenuation. Line-emission from e.g. shocked gas, is not likely to be responsible for the excess brightness because (i) Morris & Reipurth (1990) found no line-emission from the ansae, and (ii) we compute similar excesses in the brightness of the ansae in the V and I-band images obtained by Langill et al. (1994).

3.2. Millimeter-wave emission

The observed CO spectra, with linear baselines subtracted are shown in Fig. 3. The resolution is 2.7 (1.5) km s^{-1} for the 3 (1) mm lines. Small maps of the CO $J = 2 \rightarrow 1$ emission show that its angular extent is only marginally larger than the 12-13″ telescope beam, and we estimate that the full size at half maximum of the intrinsic CO $J = 2 \rightarrow 1$ brightness distribution is smaller than 10″, probably ∼ 5″. The CO spectra show a narrow central component centered at V_{LSR}=−11 km s^{-1}, with a width of ∼20 km s^{-1}. We assume that this strong feature comes from a compact, spherical component, expanding at ∼10 km s^{-1}, although it may have a flattened disk-like geometry, as found in other PPNe from direct observations (e.g. Bujarrabal et al. 1998, Sánchez Contreras et al. 1997). This component probably represents the remnant of the AGB envelope that has not been significantly accelerated by interaction with a fast post-AGB wind. We find intense wings at both sides of this spectral component; comparison with other PPNe leads us to believe that the wing emission probably arises from material in the nebular lobes expanding parallel to the long axis of the nebula. Assuming an inclination of the nebular axis to the sky plane, θ_i=15°(Roddier et al. 1995), the maximum deprojected

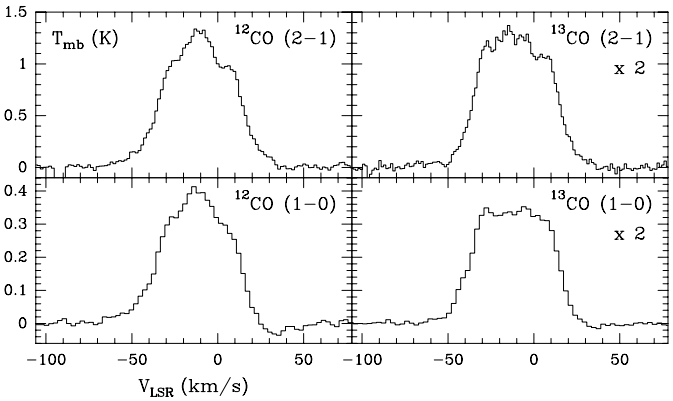

Fig. 3. CO lines observed in Frosty Leo

expansion velocity of the lobes is v_{axis} ∼190 km s^{-1}, where $v_{axis} = v/\sin\theta_i$, and v ∼50 km s^{-1}.

The intensity ratio ^{12}CO/^{13}CO for both transitions shows that the ^{13}CO transitions are optically thin (optical depth <0.5), assuming a similar rotational excitation temperature (T_{ex}) for both species. The mass, momentum and energy of the material emitting in each velocity channel can then be obtained from the ^{13}CO line profiles, taking into account that the source is unresolved (Bujarrabal et al. 1997, 2000). T_{mb} is given for every frequency by

$$T_{mb}\,\Omega_{mb} = (J(T_{ex}) - J(T_{bg})) \int k_\nu \,\mathrm{d}l\, A\,/D^2,$$

where Ω_{mb} is the main-beam solid angle, $J(T) = \frac{h\nu/k}{e^{h\nu/kT}-1}$, k_ν is the absorption coefficient, dl is the length increment along the line of sight, and A and D are, respectively, the projected area of, and distance to, the source. This equation implies that $T_{mb} \propto M_v$, where M_v is the mass moving at velocity v in the line of sight. The total mass of a kinematic component comes from integrating M_v over the appropriate velocity range.

For the spherical component expanding with constant v_{exp} (∼10 km s^{-1}), we get the "momentum" $P_c = M_c\, v_{exp}$ and the energy $E_c = M_c\, v_{exp}^2/2$, where $M_c \propto \int T_{mb}\, dv$ and the integral extends over the central spectral component's velocity range. For the fast component, each mass element M_v is assumed to be in axial expansion with v_{axis} ($\propto v$); hence $P_v \propto T_{mb}\, v_{axis}$ and $E_v \propto T_{mb}\, v_{axis}^2/2$, for every channel in the line wings (i.e. for every parcel of gas at high velocity). The scalar addition of all these momenta and energies gives the total *scalar momentum*, P_{tot}, and the energy, E_{tot}, of the fast outflow.

In our calculations we have used the ^{13}CO J=1-0 data, since for this line the optical depth is lowest and Ω_{mb} is the largest (ensuring that the source is unresolved). We have assumed a ^{13}CO/H_2 abundance ratio of 4×10^{-5} (Bujarrabal et al. 1997, Sánchez Contreras et al. 1997) and a distance of 3 kpc (see §1). The excitation temperature, T_{ex} is taken to be 10 K similar to that found in well studied PPNe, and consistent with the intensity ratio of the optically-thin ^{13}CO transitions. In addition, if we reasonably assume that the ^{12}CO lines are optically thick in the peak of the profile and that the source size is 5″, then

the peak $T_{\rm mb}$ implies $T_{\rm ex}$ $\sim$11 K. We have also carried out our computations using $T_{\rm ex}$ $\sim$15 K. In order to evaluate the uncertainty due to the poorly known geometry of the molecular outflow, we have also estimated $P_{\rm tot}$ and $E_{\rm tot}$ assuming that the high velocity emission comes from a spherical shell or a disk perpendicular to the nebular axis of the nebula. The results from all these calculations depend only slightly on the assumed geometry and excitation. The mass of the low- and high-velocity components are respectively 0.15 and 0.25 $M_{\odot}$, the momenta of the fast outflow ranges between 2 and 4.5×10^{39} g cm s^{-1}, and the kinetic energy ranges between 3.5×10^{45} and 2×10^{46} erg (for details see Bujarrabal et al. 2000). We can compare these results with the energy and momentum that the stellar luminosity can contribute per yr, L = 3×10^{44} erg yr^{-1}, L/c = 9×10^{33} g cm s^{-1} yr^{-1}. The time taken by Frosty Leo to evolve from the AGB stage to its current state must be $<$1000 yr, since 1000 yr is the ratio between the radius of ansae and the maximum velocity (190 km s^{-1}), and the ratio between the radius of the CO emitting region and this velocity is even smaller. Moreover, the wind interaction time is thought to be still much smaller. Therefore, we conclude that the maximum momentum that the stellar luminosity could have contributed during this period is a factor $\sim$ 500 smaller than that carried by the fast outflow.

Finally, we estimate from the ^{12}CO to ^{13}CO intensity ratio in the $J = 1 \rightarrow 0$ line wings (where opacity effects are likely to be small) that the ^{12}C/^{13}C isotope ratio is $\gtrsim$4. This value lies at the low end of the range for O-rich circumstellar envelopes around AGB stars.

4. Discussion and summary

The multiple jet-like features which we have found in Frosty Leo are probably the result of *past* collimated outflows interacting with its dense AGB CSE, since no emission lines from shocked gas have been observed either in the optical or near-IR (e.g. 2.1μm H_2 line, Weintraub et al. 1988). Although several PPNe have been well-resolved by HST [e.g. Roberts 22 (SZBtL99), Hen 401 (Sahai et al. 1999b), OH231.8 (Bieging et al. 2000)], Frosty Leo is only the second PPN after CRL2688 (Cox et al. 2000), and the first oxygen-rich one, which shows *direct evidence for well-focussed jets close to the equatorial plane*. Such jets were hypothesized by Sahai and Trauger (1998) to explain the morphologies seen in their sample of young PNe. The extended, knotty structure of the ansae suggests that they are the result of a polar jet which varied both its direction and intensity with time. The blobs B_N & B_S appear to be distinct, dense entities embedded inside extended tenuous bubbles (L_N & L_S), similar to those seen in Roberts 22. The creation of the blobs is thus a puzzle, since any interacting-winds mechanism would have difficulty finding sufficient matter inside the tenuous bubbles for sweeping up into the blob structures.

Our CO spectra show the presence of slow ($\sim$10 km s^{-1}) and fast ($>$50 km s^{-1}) components in the molecular outflow; the slow outflow may help in explaining the low grain velocities (4-15 km s^{-1}) observed by Dougados et al. (1992). We find that Frosty Leo has the largest ratio of the mechanical momentum in the fast outflow ($P_{\rm tot}$) to the radiative momentum (L/c) amongst PPNe (scaling $P_{\rm tot}$ for all objects to the same ^{13}CO/H_2 ratio) which, as a class, show large ratios (Bujarrabal et al. 2000). Only one other PPN, OH231.8+4.2, shows a momentum excess comparable to that of Frosty Leo. Since the CO emission comes from the inner ($<$10$''$) region of the nebula in Frosty Leo, this very energetic outflow seems to be associated with low-latitude material in the vicinity of the jets seen in the HST image. The very high mechanical momentum excess in this PPN indicates that the jets that disrupted the AGB shell, yielding the complex actual shape of the nebula, were not powered by radiation pressure. The source of this excess is probably associated with binarity, and may derive from the gravitational energy of material accreted by a compact companion. However, the separation of the binary *apparently* seen in Frosty Leo (190 AU, for a minimum distance of 1 kpc) is much too large for the formation of an accretion disk which could drive a collimated outflow.

Acknowledgements. For this work, RS was financially supported by NASA from a Long Term Space Astrophysics grant (no. 399-30-61-00-00) and grant GO-06816.01-95A from the Space Telescope Science Institute; and VB & AC were supported by the Spanish DGES, under project PB96-0104.

References

Bieging, J.H., Meakin, C.A., Kelly, D.M., Dayal, A., Latter, W.B., Hora, J.L., & Tielens, A.G.G.M. 2000, ASP Conference Series, 199, 183

Bujarrabal, V., Alcolea, J., Neri, R. & Grewing, M.: 1997, A & A 320, 540

Bujarrabal, V., Alcolea, J. & Neri, R.: 1998, ApJ 504, 915

Bujarrabal, V., Castro-Carrizo, A., Alcolea, J. & Sánchez Contreras, C.: 2000, in preparation.

Cox, P., Lucas, R., Huggins, P.J., Forveille, T., Bachiller, R., Guilloteau, S., Maillard, J.P. & Omont, A. 2000, A&A, 353, L25

Dougados, C., Rouan, D., & Lena, P. 1992, A&A, 253, 464

Forveille, T., Morris, M., Omont, A. & Likkel, L. 1987, A&A,176, L13

Langill, P.P., Kwok, S. & Hrivnak, B.J. 1994, PASP, 106, 736

Mauron, N., Le Borgue, J.-F., & Picquette, M. 1989, A&A, 218, 213

Morris, M. & Reipurth, B. 1990, PASP, 102, 446

Robinson, G., Smith, R.G., & Hyland, A.R.: 1992, MNRAS, 256, 437

Roddier, F., Roddier, C., Graves, J.E. & Northcott, M.J.: 1995, ApJ, 443, 249

Rouan, D., Omont, A., Lacombe, F., & Forveille, T.: 1988, A&A, 189, L3

Sahai, R. & Trauger, J.T. 1998, AJ, 116, 1357

Sahai, R., Zijlstra, A., Bujarrabal, V., te Lintel Hekkert, P.: 1999a, AJ, 117, 1408 (SZBtL99)

Sahai, R., Bujarrabal, V., Zijlstra, A.: 1999b, ApJ, 518, L115

Sánchez Contreras, C., Bujarrabal, V. & Alcolea, J.: 1997, A & A 327, 689

Weintraub, D.A., Huard, T., Kastner, J.H., Gatley, I.: 1988, ApJ, 509, 728